International Journal of Naval Architecture and Ocean Engineering 10 (2018) 670–682

Contents lists available at ScienceDirect

International Journal of Naval Architecture and Ocean Engineering

journal homepage: http://www.journals.elsevier.com/international-journal-of-naval-architecture-and-ocean-engineering/

Response of low-temperature steel beams subjected to single and repeated lateral impacts

Dac Dung Truong [a], Hae-Jung Jung [b], Hyun Kyoung Shin [a], Sang-Rai Cho [a, *]

[a] School of Naval Architecture and Ocean Engineering, University of Ulsan, 93 Daehak-ro, Namgu, Ulsan 44610, South Korea
[b] Hyundai Mipo Dockyard, 100 Bangeojinsunhwan-doro, Dong-Gu, Ulsan 44113, South Korea

ARTICLE INFO

Article history:
Received 26 July 2016
Received in revised form
9 September 2017
Accepted 10 October 2017
Available online 29 December 2017

Keywords:
Low-temperature steel beam
Repeated impact test
Sub-zero temperature
Numerical analysis

ABSTRACT

This paper presents the experimental and numerical investigation results of the response of low-temperature steel (LT-FH32 grade steel) beams under repeated impacts at room temperature and a single impact at a sub-zero temperature. After conducting tensile tests at room and sub-zero, repeated impact tests were conducted on two clamped single-beam models at room temperature, and single-impact tests of two other clamped single-beam models were conducted at −50 °C. The single and repeated impact tests were conducted by releasing a knife-edge striker using a drop testing machine. The permanent deflection of the model measured after each impact gradually increased with increasing number of impacts. Under the reduced temperature, the permanent deflection of the models slightly decreased. The numerical analyses were also performed to predict the damage response of the tested single-beam models. A comparison of the numerical prediction with those of experiments showed quite reasonable agreement.

1. Introduction

Recently, the Liquefied Petroleum Gas (LPG) carrier sector has emerged as a new hope in the shipping and shipbuilding industries. LPG carriers (see Fig. 1, described as a mid-cross section), unlike general cargo ships, especially with regard to the characteristics of the cargo to be transported carry the possibility of causing a serious accident in the surrounding environment by the diffusion, explosion or evaporation of leaked gas; thus, the study of the impact resistance of the primary and secondary barriers for cargo is important. However, in this paper, the study is primarily related to the secondary barrier.

Because the transportation of gas is hazardous for many reasons of potential danger such as impact resistance and various requirements mechanical properties of the steel material are regulated by the International Maritime Organization within International Gas Carriers code (IMO, 1993). To prevent the corrosion of steel used in LPG ship structures, Low-Temperature steel (LT), which has a higher amount of nickel (Ni), was considered to improve toughness at low temperature from −30 °C to −196 °C. Therefore, to preserve the LPG cargo, the evaluation of the impact resistance of hull structures such as primary and secondary barrier structures made of low-temperature steel has become important.

During its service life, ships and offshore structures including LPG carriers may be exposed to various loading conditions such as slamming, sloshing, green water and mass impacts and, especially repeated lateral impacts from ice floes and/or floating objects. It is known that plastic deformations accumulate if the structure is subjected to repeated impacts. Accumulation of permanent deformations depends on the severity of loads and the number of load repetitions in addition to the strength of the material used in fabricating the structures.

Several researchers have investigated the effect of repeated impact on steel structures (Zhu and Faulkner, 1996; Huang et al., 2000; Seifried et al., 2005; Chae, 2008; Minamoto et al., 2011; Henchie et al., 2014; Cho et al., 2014). Some of them (Zhu and Faulkner, 1996; Huang et al., 2000; Seifried et al., 2005; Chae, 2008; Minamoto et al., 2011; Cho et al., 2014) focused on repeated mass impacts, whereas others (Henchie et al., 2014) are related to repeated uniform blast loads. In Zhu and Faulkner (1996), Huang et al. (2000) and Chae (2008), unstiffened plates made of mild steel have been employed to investigate repeated impact responses at room temperature, whereas Seifried et al. (2005) and Minamoto et al. (2011) considered rod models made of DIN S235

* Corresponding author.
E-mail address: srcho@ulsan.ac.kr (S.-R. Cho).
Peer review under responsibility of Society of Naval Architects of Korea.

https://doi.org/10.1016/j.ijnaoe.2017.10.002

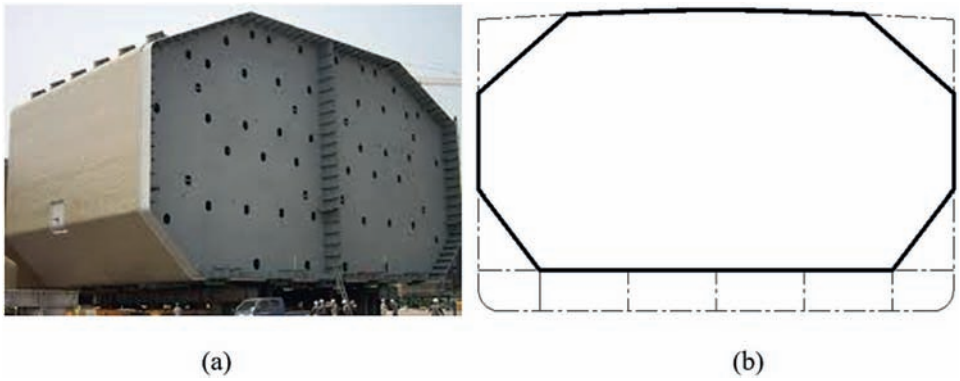

Fig. 1. Barriers of LPG tanker: (a) Primary barrier, (b) Secondary barrier.

which corresponds to JIS SM41, to study the responses of structures under repeated impacts at room temperature. However, Henchie et al. (2014) investigated the response of circular plates made of DOMEX 700 with yield strength 750 MPa to repeated uniform blast loads, and Cho et al. (2014) employed DH36 grade steel to investigate the repeated impact effect on single-beams at room and low temperatures. Little is known about whether materials or temperatures would have any significant effect on the repeated mass impact performance of structures. However, the material properties of Low-Temperature (LT) grade steel, which is widely used in LPG carriers, have not been investigated.

In a previous study (Cho et al., 2014), the dynamic plastic response of single steel beams to repeated low-velocity impacts was primarily investigated. The repetition of impacts has relevance in applications where multiple impact sequences may be exposed to ice floes or floating objects.

The purpose of this study is to investigate the effects of single and repeated lateral impacts on the response of beams representing a stiffener with an associated plate of the secondary barrier of an LPG carrier. Repeated impact tests were conducted on four beams made of low-temperature steel (LT-FH32 grade). Seven identical impacts were repeated for two models at room temperature, and a single-impact was applied at a sub-zero temperature (−50 °C) to the other two. Both ends of the models were fully clamped onto a strong bed during impacts. The permanent deflections were measured after each impact test. To estimate the damage of the tested models the numerical analyses were conducted using the commercial ABAQUS/Explicit software package. In the numerical model, both strain and strain rate hardenings were considered. The strain hardening was determined using the stress-strain relationships obtained from the tensile tests performed in this study. However, the strain rate hardening was determined by adopting the Cowper and Symonds strain rate hardening model along with the material constants provided by the literature. Reasonable agreement has been achieved between the experimental results and numerical predictions.

2. Experimental investigations

2.1. Material properties

To obtain the mechanical properties of the test model material at various temperature conditions, two series of tensile tests were conducted. The tensile tests at room temperature and sub-zero temperatures (−30 °C, −50 °C and −70 °C) were performed using the universal testing machines of the University of Ulsan and of Mokpo National University of Korea, respectively. The material tested in this study was low-temperature steel of LT-FH32 grade.

Five tensile test coupons were cut from each parent plate to fabricate the test models, which were then machined and their dimensions were measured before testing. For the tensile testing at low temperature, a cold chamber had been installed in the universal testing machine. Both tensile tests were conducted at a rate of 1.0 mm/min by displacement-control until fracture occurred to eliminate the dynamic effects. The force–elongation curve, which was used to determine the engineering stress-strain relationships of the materials, was recorded. The test procedures satisfied the requirements of the Korean Standard (KS, 2007). The average mechanical properties obtained by tensile tests at room and sub-zero temperatures are summarized in Table 1. In Table 1, t is the thickness of the coupon, σ_Y is the yield strength, σ_T is the ultimate tensile strength, E is the Young's modulus, ε_{HS} is the hardening start strain, ε_T is the ultimate tensile strain, and e_F is the fracture strain. Fig. 2 shows the engineering stress–strain curves of the model materials as well as its true values at various temperature conditions.

From the testing results, it is noticed that the material at low temperature became harder than that at room temperature. In particular, the yield strength increases by approximately 5.4–6.7% at −30 °C, by 10.5–12.4% at −50 °C, and by 13.3–17.8% at −70 °C, whereas the tensile strength increases by approximately 6.2–7.6% at −30 °C, by 10.9–11.2% at −50 °C, and by 13.3–14.9% at −70 °C, compared with those at room temperature, as shown in Fig. 3. Additionally, the increasing trends of strain were also detected clearly, as illustrated in Table 1, which increased gradually with decreasing temperature.

2.2. Test models

Four single beams were fabricated for the impact tests. Two models denoted LT-R1 and LT-R2 were tested at room temperature, whilst the other two labelled LT-L1 and LT-L2 were tested at approximately −50 °C. The web and flange of the beam were cut from low-temperature steel sheets of 13 mm in thickness and welded to endplates and brackets at the ends of the beam which were cut from low-temperature sheets of 10 mm thickness. The endplates have the bolt holes, which were bolted to the support fixtures. The nominal thicknesses and dimensions of the test model are depicted in Fig. 4(a) and a fabricated model, model LT-R1, is shown in Fig. 4(b). After fabricating the models, grid lines were marked with 25 mm spacing from the mid-length of the beam. The initial imperfections of the beam were carefully measured using a laser gauge before being mounted on the testing frame.

Table 1
Mechanical properties of the test model material at room and sub-zero temperatures.

Part of model	Temp. [°C]	T [mm]	σ_Y [MPa]	σ_T [MPa]	E [MPa]	e_{HS} [-]	e_T [-]	e_F [-]
Web and flange of beam	RT	13.44	365.0	464.5	206,000	0.0247	0.1928	0.4263
	−30		389.5	499.7	206,000	0.0244	0.1984	0.5027
	−50		410.1	516.6	206,000	0.0279	0.2088	0.4889
	−70		430.0	533.5	206,000	0.0306	0.2090	0.4987
End plate and bracket	RT	10.39	372.8	482.5	206,000	0.0205	0.1785	0.3908
	−30		392.8	512.5	206,000	0.0221	0.1871	0.4473
	−50		411.8	534.9	206,000	0.0252	0.1906	0.4447
	−70		422.5	546.7	206,000	0.0256	0.1926	0.4523

Note: RT denotes room temperature.

2.3. Experimental set-up

The single and repeated impact tests were conducted at −50 °C and room temperatures, respectively, using drop testing machine shown in Fig. 5(a). This machine has been successfully employed in single impact tests and repeated impact tests for unstiffened plate (Chae, 2008), unstiffened tubular structures (Cho et al., 2013), small-scale tanker double-hull structures (Cho et al., 2011), beam structures (Min et al., 2013; Cho et al., 2014) and ring-stiffened cylinders (Cerik et al., 2015). The header of the striker was a knife-edge type with a width of 400 mm (see Fig. 5(b)). The mass of the striker was 298 kg for all impact tests.

The experimental procedure used in this investigation is generally similar to that used in the previous study (Cho et al., 2014). However, in the previous study, Cho et al. (2014) released the boundaries between impacts to conveniently measure the permanent deflections of the tested model. This may have led to damage far less due to elastic spring-back of the beam. In fact, ships and offshore structures will not be released between repeated impacts, which are different from the test condition in that study. In the current study, therefore, the models were firmly fixed at both ends of the model to the fixtures and strong bed of the drop testing machine by bolting throughout all impacts to realistically reflect marine structure impact problems.

Seven impacts were carried out for the models LT-R1 and LT-R2 with the same boundary conditions by dropping the striker repeatedly from the same drop height with the same mass of the striker. Nevertheless, the models LT-L1 and LT-L2 were tested only for a single-impact event with the same impact conditions as those of the room temperature tests.

To obtain strain history information, twelve strain gauges were glued to each model and the arrangement of the strain gauges can be found in Fig. 6(a). Strains were recorded 10,000 times per second, using amplifiers and an A/D converter.

For the sub-zero temperature tests, to reduce the temperature for the cold models, cold chambers were fabricated with Styrofoam panels and were glued onto the models covering the middle parts. The cold chamber was filled with dry ice and ethanol. Before filling the cold chamber four thermocouples were glued onto the flat stiffener of the model to measure the temperature. The thermocouples were arranged as shown in Fig. 6(b). The model was kept in the cold chamber for approximately 112 min. The temperature histories measured are shown in Fig. 7. As seen in the figure, approximately 10 min after the cooling was started, the temperature of the chamber reached approximately −76 °C and this temperature was maintained. Before conducting the impact drop test the chamber was removed from the model. When the temperature increased to approximately −50 °C, the striker was released from the magnet and subsequently impacted the model.

The impact location was the mid-length of the beam. After hitting the model, the striker rebounded with no control of its motion. To protect the model from further damage by the rebounded striker, the surface of the beam except for the impact zone was covered with a 5 mm thick rubber pad. As result of the rebound velocity of the striker after each impact event, the immediately successive second impact with a small sub-drop height of the striker was observed visually. It should be noted that its effect on the final deformed shape of the model was insignificant. For this reason, the successive second impact would be neglected in the finite element simulations. After each impact, the permanent deflection of the model is measured without releasing the bolts using the laser gauge. The striker is set at the same predefined height for the subsequent impacts of the repeated impact tests. The next impact was set and the next measurement was then started again. Thus, the striker impacts the same (now deformed) contact area again with the same initial velocity. Table 2 presents the collision conditions of all tests as well as the measured and predicted permanent deflections.

2.4. Impact test results

The deformed shapes of the tested models are shown in Fig. 8. The V-shaped deformation with plastic hinges at the impact position and the supports are clearly detected in both single impact and repeated impacts cases.

The maximum permanent deflections around the mid-length of the tested models are presented in Table 2. For the single impact, the test models showed more deflection at room temperature by approximately 18.2% at an impact velocity of 3962 mm/s and 5.9% at 3132 mm/s compared with those at −50 °C. It may be concluded that the structures under impact loading at low temperature can be stiffer than those at room temperature. This is because, as indicated in Sub-section 2.1, both yield strength and ultimate tensile strength increased at low temperatures, which results in decreased permanent deflection compared with that at room temperature. For repeated impacts at room temperature, the gradual increase in maximum permanent deflections of the tested models can be clearly observed with the number of impacts, whilst the increment of the maximum permanent deflections of the tested models slightly decreased regardless of impact velocity. However, a faster decrease in the increment of maximum permanent deflections can be detected in the case of a lower impact velocity compared with that at a higher velocity of impact.

The strain measurements of the tested models provided more details to understand the deformation process of the model during impact. The strain histories are illustrated in Fig. 13 for the first impact of model LT-R2. According to the strain measurements at position 3 and 4, the flange of the beam was mainly in the longitudinal direction owing to high membrane tension, whereas in the transversal direction the strain was compressive. In addition, the strain in the transversal direction approached its permanent value earlier than in the longitudinal direction.

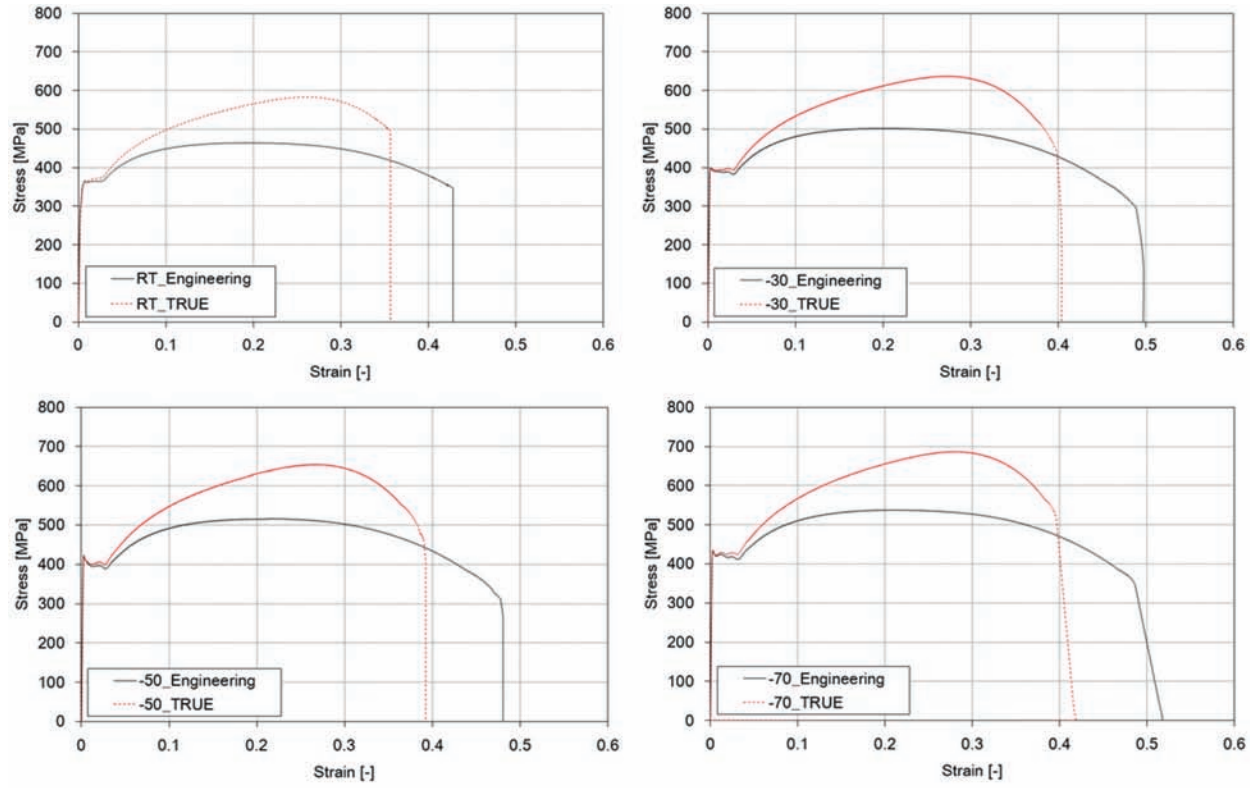

(a) Web and flange

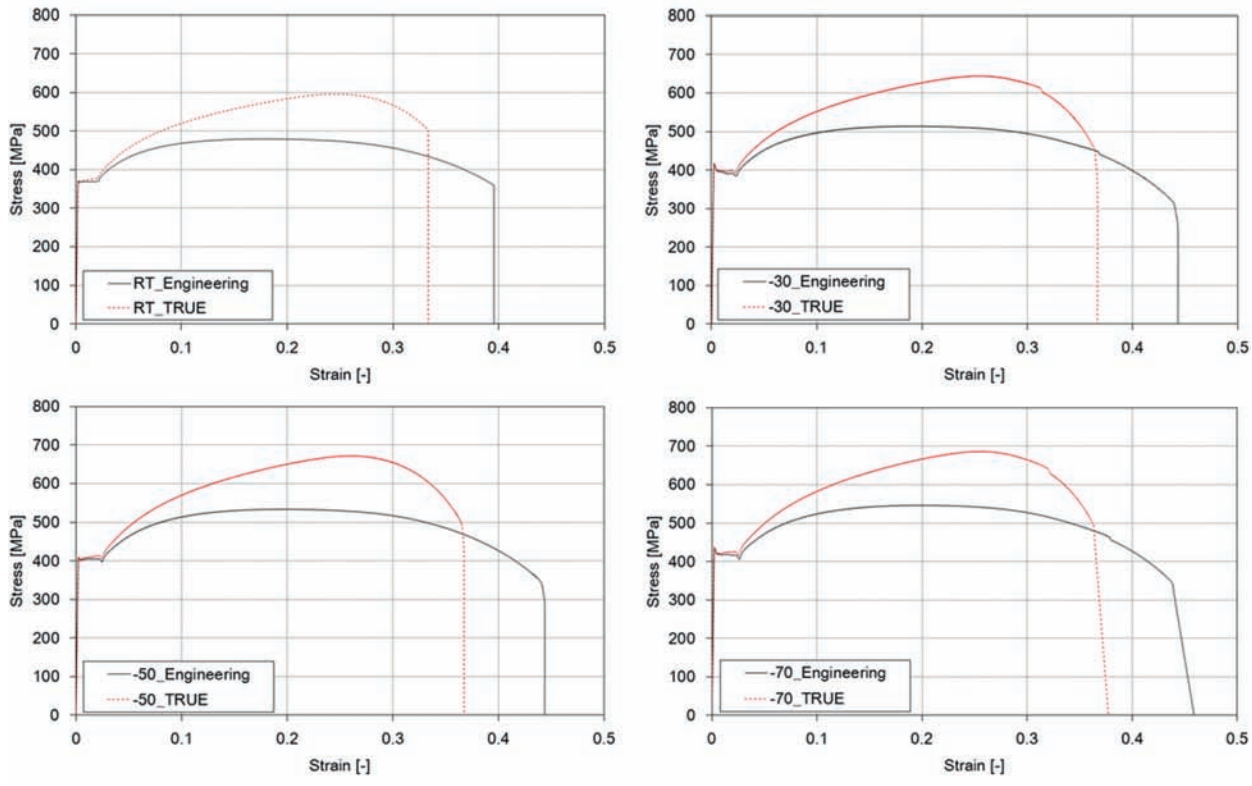

(b) End plate and bracket

Fig. 2. Engineering and true stress–strain curves of model materials.

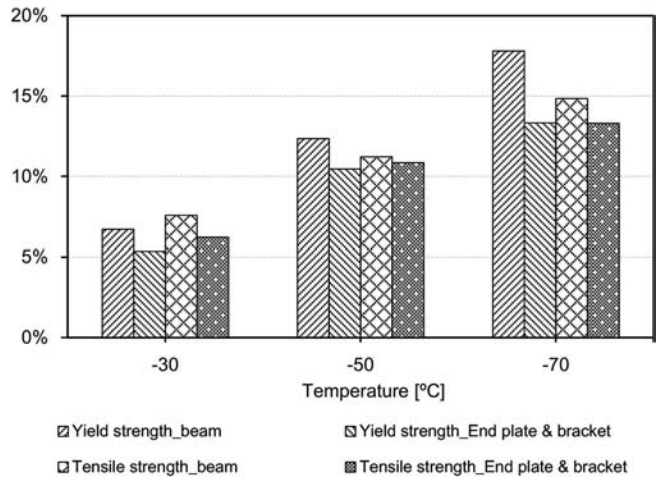

Fig. 3. Effect of temperature on yield and tensile strengths.

3. Numerical investigations

3.1. Finite element modelling

The numerical model of the low-temperature single beam under single and repeated mass impacts was developed using the commercial finite element software package ABAQUS/Explicit (ABAQUS, 2010). The numerical model designed consists of a single beam with end-plates and fixtures and a striker as shown in Fig. 9(a), which are the same as in the experiment in terms of dimensions and material properties of the test model and mass of the striker.

The numerical model was meshed using four-node shell elements with a reduced integration scheme (S4R), and hourglass control and finite membrane strains were used. Thickness integration was performed using the Simpson rule with five integration points through the thickness. The striker was modelled as a rigid body using the R3D4 element. All types of element formulations are the default in ABAQUS/Explicit.

To obtain accurate and reliable numerical results and reduce the time of analysis, convergence tests were performed. After the

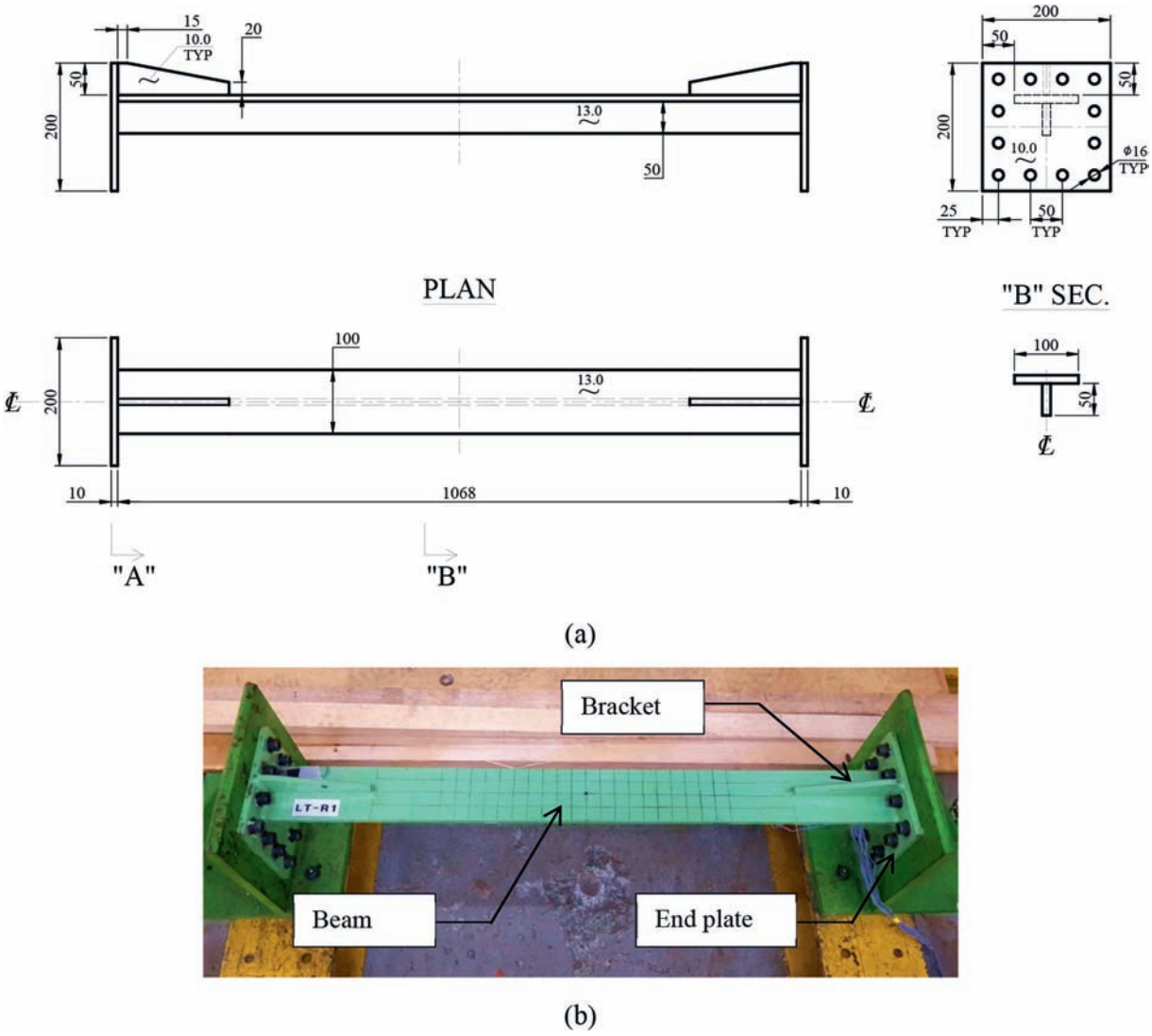

Fig. 4. Test model: (a) dimensions, (b) fabricated model.

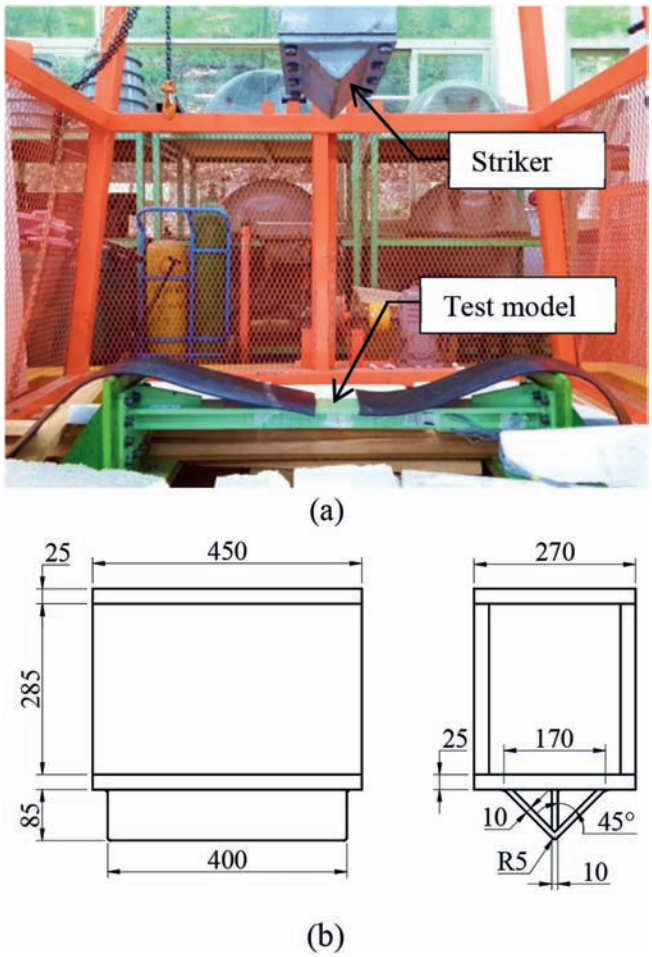

Fig. 5. Drop testing machine: (a) test model in position, (b) details of striker.

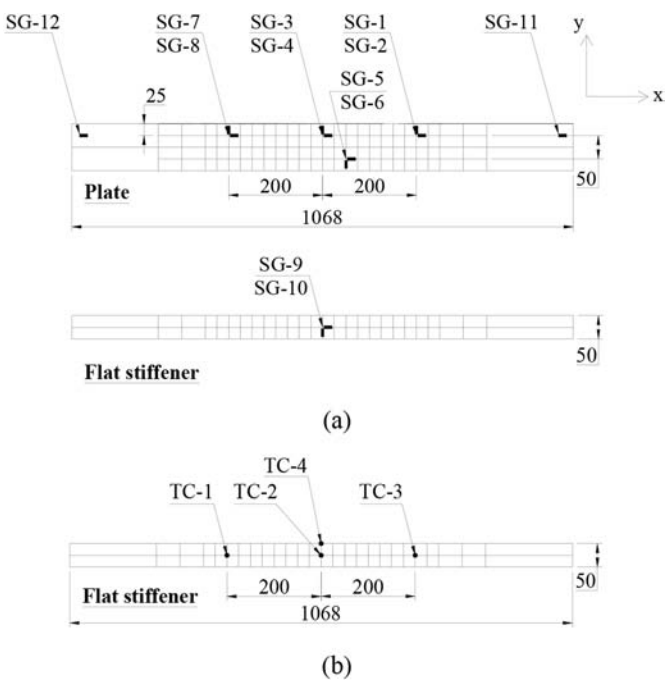

Fig. 6. Arrangement of (a) strain gauges and (b) thermocouples.

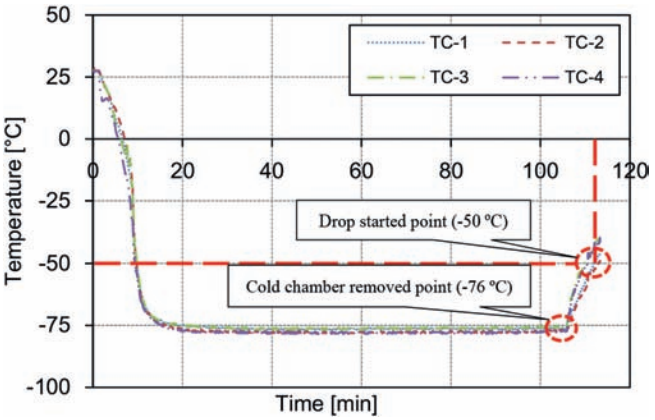

Fig. 7. Temperature history measured by thermocouples.

convergence tests, a properly sized finite element mesh was adopted in each model. The contact zone of the model with the striker was modelled with fine meshes, 2 mm × 2 mm. The size of the elements far from the contact zone was 5 mm × 5 mm. Some median mesh sizes were used in the transition regions as shown in Fig. 9(b). The FE representation of the support fixtures was used to simulate the experimental clamped boundary conditions of the single beam and striker using a relatively coarse mesh of shell elements with a side length of approximately 20 mm.

To provide an accurate representation of the experimental support and simplify the numerical model, part of the supporting structures is modelled as a fixture shown in Fig. 9(a). The fixtures were fully fixed (Ux, Uy, Uz, Rx, Ry, Rz = 0) at four bottom bolt holes and the inside part of the base of the fixtures were fixed in the vertical direction (Uz = 0) to simulate the experimentally clamped boundary conditions of the beam. For the striker, the mass and velocity were applied to the reference points shown in Fig. 9(a) to simulate the expected impact energy for the impact problem. It is noted that the motions of the rigid striker were governed by the motions of the reference points by assigning the initial collision velocity for the reference point in the vertical direction.

3.2. Contact relationships

Because no bolt connection fracture was observed in the impact test, the “Tie” constraints were used to simulate the fully-bolted connections between endplates linked to the beam and the fixtures. This algorithm of constraint makes the translational and rotational degree of freedom the same as for the pairs of surfaces. A “surface-to-surface” contact was defined in the numerical model. The penalty and ‘hard’ contact methods were used to define the tangential and normal interaction behaviour of the possible self-contact among the parts of the model during impacts, and the friction coefficient between the endplate and the fixture and between the flange of the beam and the striker was set to be 0.2 (Villavicencio and Guedes Soares, 2011).

3.3. Material properties definitions

The definition of the model material is most important, so the mechanical properties of the material used in the numerical model are obtained from the series of tensile tests conducted as described in the previous section. Because the engineering stress–strain curve does not give a true indication of the deformation characteristics of a metal, it is necessary to use the true stress–strain curve representing the basic plastic-flow characteristics of the

Table 2
Test conditions, experimental results and the predictions.

Model	Striker				Results, δ_{max}		
	Imp.	Drop height [mm]	Mass of striker [kg]	Initial velocity [mm/s]	Exp. [mm]	Num. [mm]	Ratio (Num./Exp.)
LT-R1	1st	800	298	3961.8	26.0	26.15	1.01
	2nd				43.0	43.06	1.00
	3rd				56.0	54.41	0.97
	4th				70.0	63.35	0.91
	5th				84.0	71.01	0.85
	6th				94.0	77.73	0.83
	7th				104.0 (108.0[a])	83.81	0.81
LT-R2	1st	500		3132.1	18.0	16.72	0.93
	2nd				28.0	29.41	1.05
	3rd				37.0	38.74	1.05
	4th				44.0	45.37	1.03
	5th				50.0	50.48	1.01
	6th				57.0	54.61	0.96
	7th				64.0 (66.0[a])	58.09	0.91
LT-L1	1st	800		3961.8	22.0 (21.0[a])	23.83	1.08
LT-L2	1st	500		3132.1	17.0 (15.0[a])	14.94	0.88

Note:
[a] After releasing boundaries.

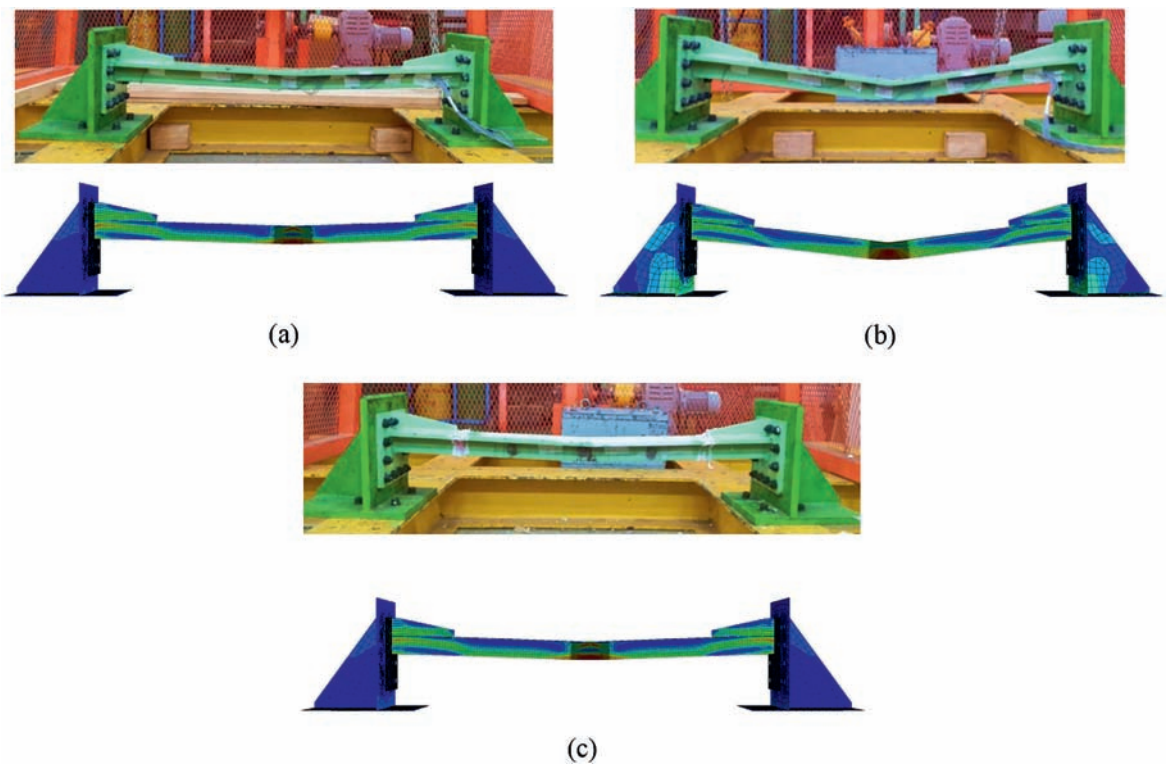

Fig. 8. Comparisons of the deformed shape profile of the tested models with the predictions: (a) after the 1st impact and (b) after the 7th impact at room temperature (model LT-R2), (c) after single impact at −50 °C (model LT-L2).

material (Dieter, 1986). Thus, the engineering stress–strain curve obtained from the standard tensile coupon test was used and converted into the true stress–strain curve, as shown in Fig. 2. In this study, however, the isotropic hardening model was simply applied based on the monotonic tensile test performed in the current study. The adequacy of applying this isotropic hardening model for repeated impact simulations was confirmed by Minamoto et al. (2011) and Henchie et al. (2014).

The true stress σ_{tr} and the true strain ε_{tr} are expressed in terms of the engineering stress σ and the engineering strain ε (Dieter, 1986).

$$\sigma_{tr} = \sigma(\varepsilon + 1) \tag{1}$$

$$\varepsilon_{tr} = \ln(\varepsilon + 1) \tag{2}$$

For the supported fixture material using DH36 grade steel (yield strength 385.1 MPa, ultimate tensile strength 552.1 MPa and Young's modulus 206,000 MPa), because the exact engineering stress–strain curve is not available, the constitutive model presented by Cho et al. (2015) was used herein to determine the corresponding strains as well as to construct the true stress-true plastic strain curve for the nonlinear analysis in ABAQUS/Explicit. It

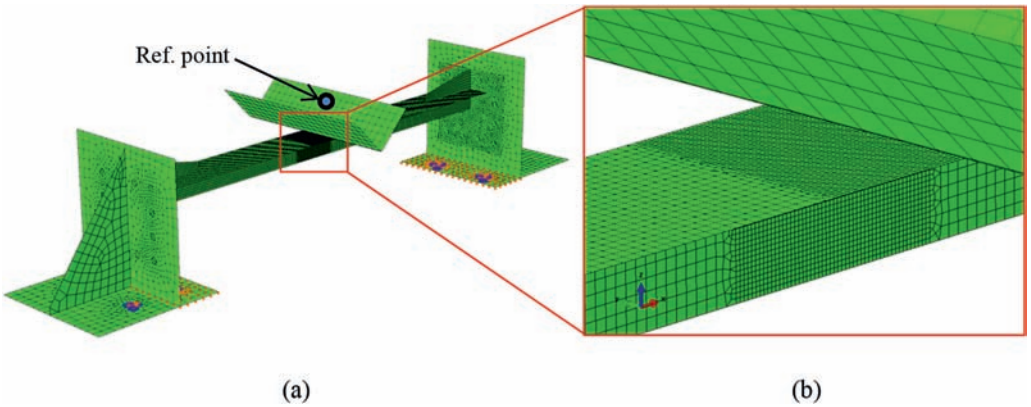

Fig. 9. Finite element model for numerical simulations: (a) 3-D view, (b) close-up view at impact area.

is noted that the true values were calculated using Eqs. (1) and (2).

$$\varepsilon_T = \varepsilon_Y \exp\left[-11.57(E/1000\sigma_Y)^2 + 15.13(E/1000\sigma_Y) - 0.191\right] \tag{3}$$

$$\varepsilon_{HS} = \varepsilon_Y \exp\left[0.762(\varepsilon_T/\varepsilon_Y)^{0.254}\right] \tag{4}$$

By substituting the stresses and strains obtained from Eqs. (1)–(4) into Eqs. (5)–(7), the constitutive equation can be obtained considering the yield plateau and the strain hardening. Figs. 2 and 10 show the true stress–strain curve used in the analyses, which were implemented in ABAQUS/Explicit as tabulated data.

$$\sigma_{tr} = E\varepsilon_{tr} \quad \text{when } 0 < \varepsilon_{tr} \le \varepsilon_{Y,tr} \tag{5}$$

$$\sigma_{tr} = \sigma_{Y,tr} + (\sigma_{HS,tr} - \sigma_{Y,tr})\frac{\varepsilon_{tr} - \varepsilon_{Y,tr}}{\varepsilon_{HS,tr} - \varepsilon_{Y,tr}} \quad \text{when } \varepsilon_{Y,tr} < \varepsilon_{tr} \le \varepsilon_{HS,tr} \tag{6}$$

$$\sigma_{tr} = \sigma_{HS,tr} + K(\varepsilon_{tr} - \varepsilon_{HS,tr})^n \quad \text{when } \varepsilon_{HS,tr} < \varepsilon_{tr} \tag{7}$$

where

$$n = (\varepsilon_{T,tr} - \varepsilon_{HS,tr})\frac{\sigma_{T,tr}}{\sigma_{T,tr} - \sigma_{HS,tr}} \tag{8}$$

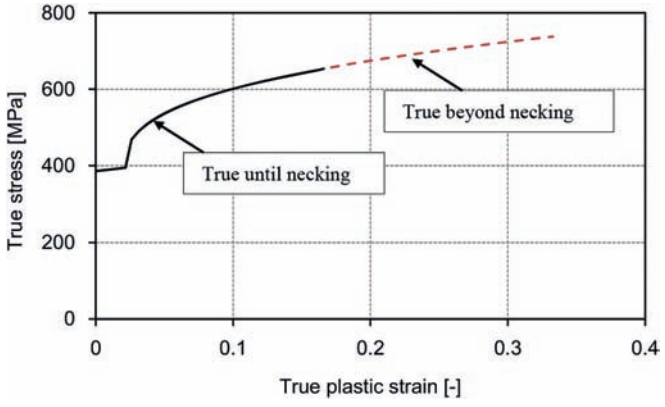

Fig. 10. True stress–strain curve of the fixture applied in the current simulation.

$$K = \frac{\sigma_{T,tr} - \sigma_{HS,tr}}{(\varepsilon_{T,tr} - \varepsilon_{HS,tr})^n} \tag{9}$$

where σ_Y is the engineering yield strength; σ_T is the engineering ultimate tensile strength; $\sigma_{HS,tr}$ is the true hardening start stress; $\sigma_{T,tr}$ is the true ultimate tensile strength; ε_T is the engineering ultimate tensile strain; $\varepsilon_{HS,tr}$ is the true hardening start strain; $\varepsilon_{T,tr}$ is the true ultimate tensile strain.

It is noted that the true stress-strain relationship beyond necking is better represented by Eqs. (7)–(9) for the model and fixture because Eqs. (1) and (2) is applicable only until the maximum load. The similar method for the material definitions has been reliably applied for impact simulation of steel structures in many studies (Villavicencio and Guedes Soares, 2012a, 2012b, 2013; Liu et al., 2013).

In addition, because the yield strength of steel under dynamic loading is sensitive to strain rate, the dynamic flow stress of steel increases with increasing strain rate. The Cowper–Symonds constitutive equation (Cowper and Symonds, 1957) widely used for structural impact problems is used here to simulate the strain-rate sensitive behaviour of the beams under repeated impact loadings. The Cowper–Symonds constitutive equation is expressed as follows:

$$\sigma_{YD} = \sigma_Y\left[1 + (\dot{\varepsilon}_p/D)^{1/q}\right] \tag{10}$$

where σ_{YD} is the dynamic yield stress at a uniaxial plastic strain rate, σ_Y is the associated static yield stress, $\dot{\varepsilon}_p$ is the equivalent strain rate and D and q are material constants for a particular material. These constants provide a reasonable estimate of the dynamic flow stress recorded during many dynamic, uniaxial and constant strain rate tests on a specific material.

It should be noted that because the models were not loaded until fracture in the experiments, only hardening curve, as well as no failure models to simulate fracture were incorporated in the current simulations.

Because the actual experimental program did not include dynamic tension tests to determine the material constants in Eq. (10), their magnitudes are obtained from the literature. Eq. (11) is the formula to estimate the material constant D (Lee and Kim, 2007) and the material constant q was assumed to be 5. It is noted that the unit of σ_Y in this equation is MPa.

$$D = \begin{cases} 92000 \exp\left(\frac{\sigma_Y}{364}\right) - 193779 & for\ \sigma_Y > 271 \\ 40 & for\ \sigma_Y \leq 271 \end{cases} \quad (11)$$

In the numerical model, Rayleigh damping was also applied to overcome the elastic vibrations, which were caused by impact and quickly approached a static equilibrium state. Rayleigh damping consists of mass proportional Rayleigh damping, α, which damps the low frequencies, and stiffness proportional Rayleigh damping, β, which damps the higher frequencies (ABAQUS, 2010). The former is used herein to include a damping matrix in the dynamic analysis which is obtained by multiplying the mass matrix of the system with the coefficient α. The coefficient α was set as the lowest natural frequency of the model (it can be the most prominent modes at which the beam will vibrate) which was obtained using a modal analysis.

3.4. Repeated impact scenario

The repeated impacts were simulated by performing the calculations repeatedly. After each impact, simulation of the artificial material damping was introduced in the model, and the calculation was then performed until all residual vibration of the model disappears. The same initial velocity was then given to the striker to simulate the later impacts, and the next impact simulation was started again until the seventh impact. In each of the restarted analyses, the deformed shape, residual stresses and strain in the current model due to the previous impact were preserved by editing the predefined field function of ABAQUS/Explicit (ABAQUS, 2010) with the initial state field applied.

4. Results and discussion

4.1. Damage evolution

Fig. 8 shows the comparisons between the experimental results and predictions in terms of the damage modes of a single steel beam subjected to repeated impacts at room temperature and a single mass impact at a sub-zero temperature with different impact velocities. A quite similar deformation shape simulations were achieved comparing with those of test results.

Fig. 11 shows the comparison of the maximum permanent deflections against the number of impacts between the simulation and the test results. In general, the numerical results demonstrate reasonable agreement with the experimental impact response, especially to the lower impact velocity model (LT-R2, 3132 mm/s) as well as the first three impact events of model LT-R1. The discrepancy during the last four impacts as depicted in Fig. 11 for the model with a higher impact velocity (LT-R1, 3962 mm/s) may be attributed to the modelling of the bolt connections using only simplified tie constraint which has the higher stiffness than that of the real bolt. It is clear that when the model under higher impact velocity, some tension of the bolt and deformation of the structural base were experimentally detected while using simplified boundary conditions (without the bolts and structural base) shown no deformation at the bolt connections (see Fig. 12(a)). It is also apparent from Fig. 11 that the increment of maximum permanent deflections gradually decreased with increasing number of impacts. Moreover, it can be seen from Table 2 that the maximum permanent deflections of the tested models at the first impact clearly decreased when the temperature decreased owing to the higher mechanical properties of models at lower temperatures.

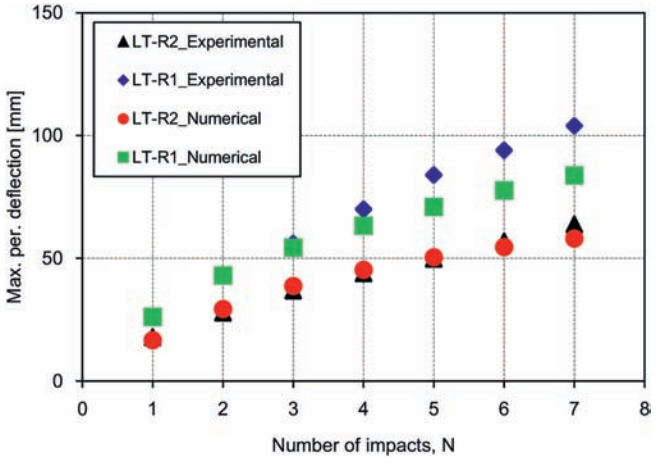

Fig. 11. Maximum permanent deflection of models against the number of impacts.

4.2. Strain history

The strains were measured during drop tests in the two room temperature tests. Fig. 13 shows the longitudinal and transversal strain histories of model LT-R2 in the vicinity of the impact location for the first impact obtained experimentally and numerically. It can be seen that the strain histories of the numerically and experimentally obtained are reasonably consistent, whereas the transient values show a somewhat different tendency except for that of SG-4.

4.3. Collision force

Considering the larger uncertainty in the impact tests compared with that of the static experiment, reasonable agreement has been achieved in this study. After substantiating the numerical analysis method of this study, further numerical analyses were conducted to investigate the effects of repeated impacts on the response of beam structures at room and sub-zero temperatures.

Fig. 14 shows the simulated collision force for a series of seven repeated impacts with 3132 mm/s for model LT-R2. The first impact yields the lowest maximum contact force and the longest impact duration. As the number of impacts increases, the maximum contact force increases but the impact duration decreases significantly. In other words, when the number of impacts increases the material can recover the elasticity, which was already confirmed by Huang et al. (2000) and Cho et al. (2014).

4.4. Rebound velocity of striker

The velocity histories of the striker are depicted in Fig. 15, which shows the increase in the rebound velocity depending on the increase in the number of impacts. Accordingly, the increase in the rebound velocity indicates the increased accelerations and collision forces.

5. Parametric study

5.1. Effect of impact locations

The deformed shapes of a beam impacted at different locations along its length are depicted in Fig. 16. In the numerical investigations the mass and impact velocity of the striker were assumed to be 298 kg and 3132 mm/s, respectively. Fig. 17 shows the effects of impact locations on the evolutions of the permanent deflections at the mid-length of the model. The impact location varies 100 mm from the mid-length towards the vicinity of the

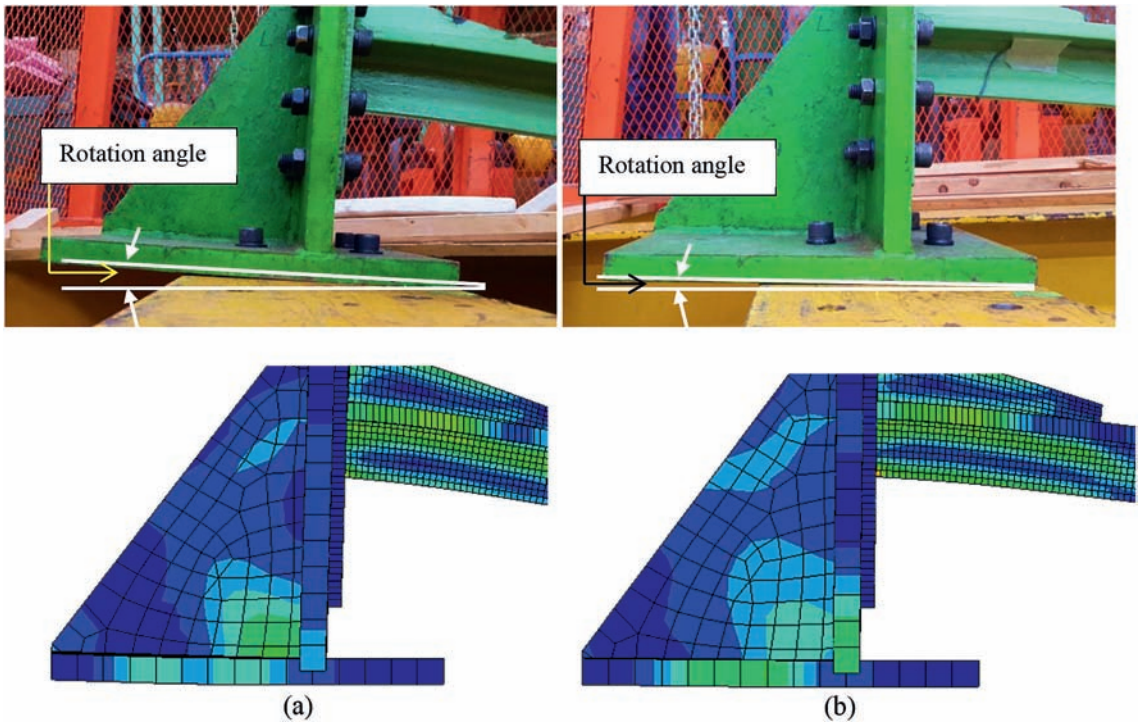

Fig. 12. Rotation of the end plate of the model after the sixth impact: (a) model LT-R1, (b) model LT-R2.

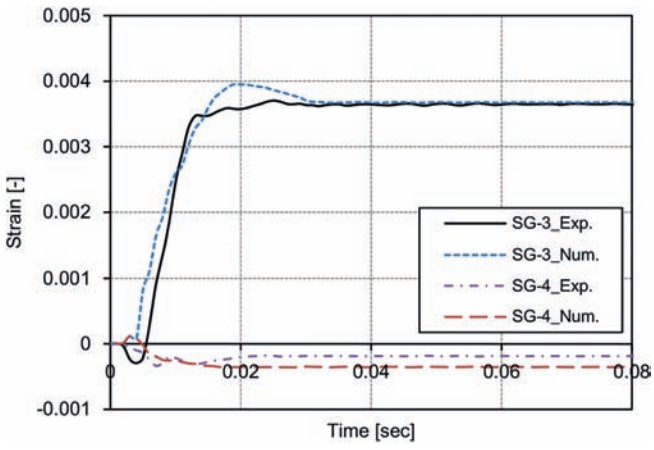

Fig. 13. Strain history of model LT-R2 throughout impacts.

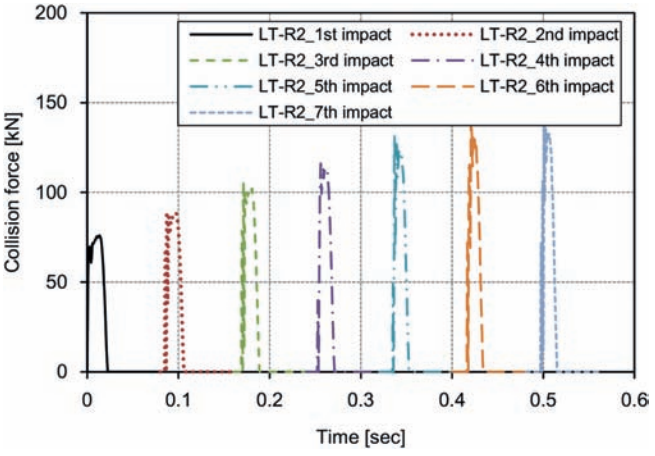

Fig. 14. Collision force histories of seven impacts of model LT-R2.

support. It can be observed that there are smaller deflections when the impact position is near the supports. It may indicate that in the initial design stage the mid-length impact can be considered.

5.2. Effect of boundary conditions

The endplate and the fixture may not dissipate a significant amount of energy. However, their effect on restraining the axial displacement and rotation of the beam affects the membrane resistance of the beam. To clarify this issue, the effect of idealizing the boundary conditions is assessed by comparison with the fully modelled experimental conditions. Three types of boundary conditions as shown in Fig. 18 were considered: (case 1) the beam was fully fixed at its ends; (case 2) the test model was modelled as a beam with endplates in which all bolt holes of the endplates were fully fixed; (case 3) the test model was modelled as a beam with endplates and fixtures in which all bolt holes of the base of the fixture were fully fixed. It is noted that shell elements were used for all cases and tie constraints were applied to model the bolt connections between the endplate and the fixture. A comparison is made for the impact conditions of LT-R2. The maximum permanent deflection against the number of impacts is shown in Fig. 19.

Case 3 (full model) approximates the experimental plastic response well, and the other cases are less accurate. For cases 1 and 2, very similar results were obtained for the first impact, but for repeated impacts in terms of maximum permanent deflection prediction, they do not give better predictions than the cases 3. Again, for both cases 1 and 2 - beam only and beam with endplate - the deflections reached throughout seven impacts are generally underestimated by the numerical models. Generally, case 3, which closely represent the actual case gives the best prediction of this point except for the last two impacts owing to the higher stiffness

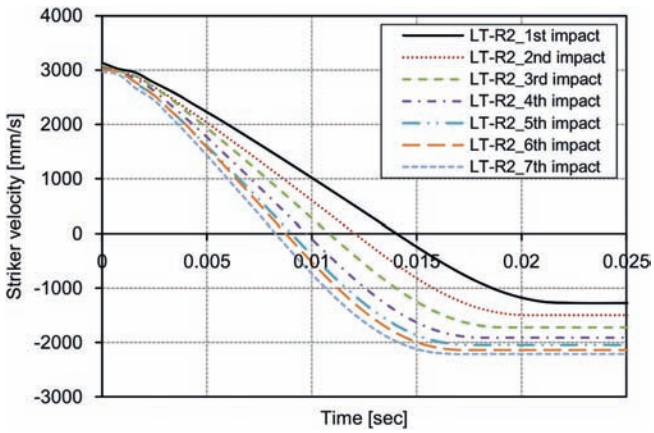

Fig. 15. Velocity histories of striker for seven impacts of model LT-R2.

of the fixture and the limitation of the tie constraint simulating the connections between the fixture and the endplate.

It is concluded that the effect of the boundary conditions on any finite element analysis for repeated impact problems should be considered as very important. The definition of the boundary conditions cannot be a rigid clamp at the ends of the model because the experimental set-up cannot be represented in a perfectly fully clamped condition, especially for repeated impact loadings applied where the experimental supports have a strong effect on the results.

5.3. Effect of strain-rate hardening definition

It is known that the definition of strain rate hardening is important and can be also an error source in numerical predictions of impact dynamic problems, thus consideration of strain rate effect through choosing material constant coefficients in the Cowper-Symonds equation, Eq. (10), can be numerically discussed. For Cowper-Symonds equation, the commonly used coefficients are $D = 40.4\ s^{-1}$ and $q = 5$ for mild steel, $D = 3200\ s^{-1}$ and $q = 5$ for high tensile steel and D can be also calculated using Eq. (11) and $q = 5$, as mentioned in Section 3.3. Recently, Choung et al. (2013) proposed Eq. (12) for prediction of the Cowper–Symonds constant D as a function of strain rate and true plastic strain. It should be noted that since the exact coefficients of determination D for the current low-temperature steel (LT-FH32) is not available, the coefficients proposed for the similar material, namely EH36 grade steel, as in Table 3, were appropriately assumed for the current single beam model.

$$D = \alpha + \beta\varepsilon_p^2 \tag{12}$$

where α and β are the coefficients as give in Table 3, and ε_p is the true plastic strain.

Fig. 20 shows the numerical investigation results of how the strain-rate hardening definitions affect the permanent deflection of a repeatedly impacted beam, the tested model LT-R2. The actual

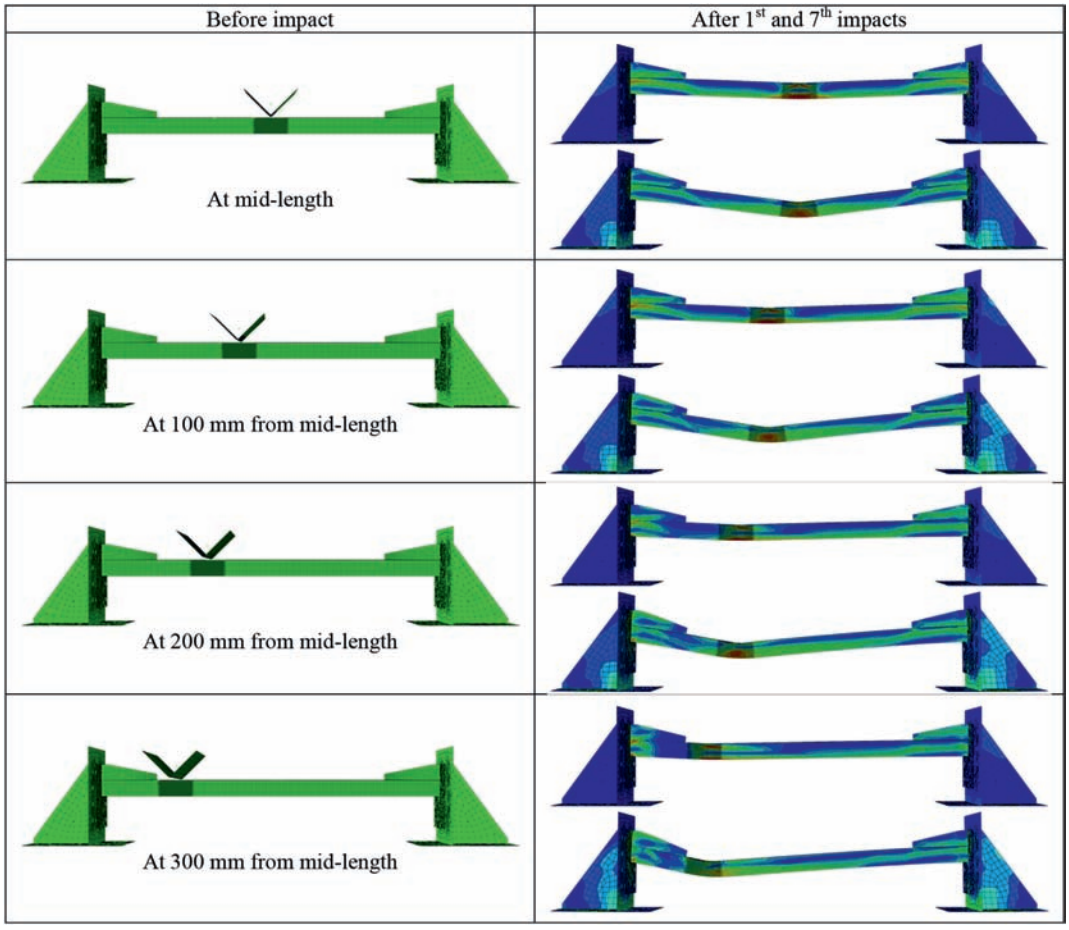

Fig. 16. Different impact locations and corresponding deformed shapes of the model.

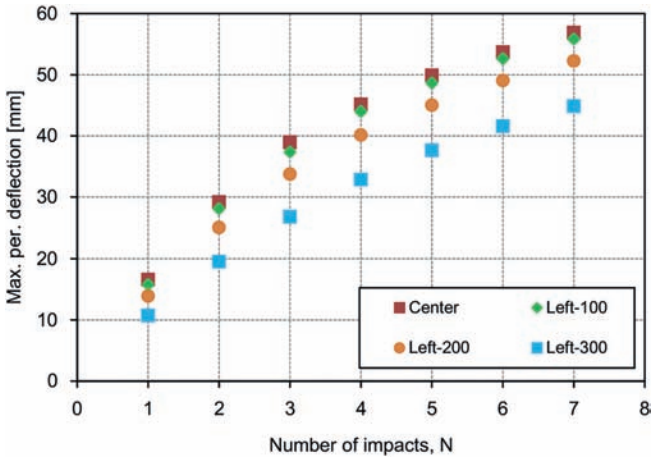

Fig. 17. Effect of impact locations on the maximum permanent deflection of models.

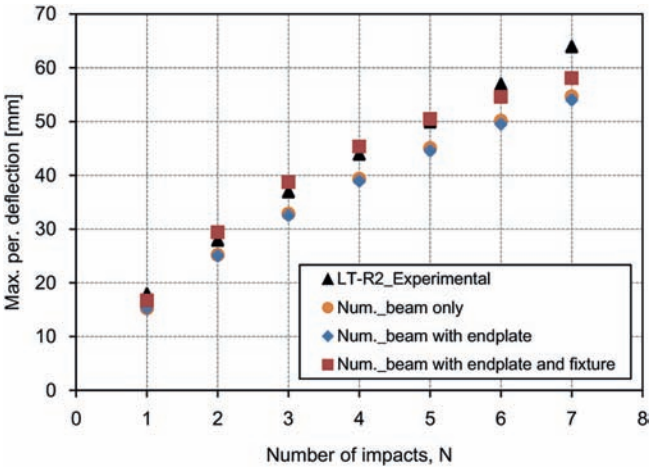

Fig. 19. Effect of boundary conditions on a maximum permanent deflection of the models.

maximum permanent deflections that were obtained in the test are also shown in the figure for comparison. It is evident that the tendencies of overall response are not affected significantly by the strain-rate hardening definitions. However, underestimation of deflection was observed for all impact events, and the maximum permanent deflection and its increment were considerably decreased when the method of predicting D proposed by Choung et al. (2013) was applied. It is apparent that for the cases using D proposed by other researchers, the maximum permanent deflection slightly depends on the selected constant D which slightly increases or decreases the stiffness of the model.

Table 3
Coefficients for determination of Cowper–Symonds constant D (/s), at room temperature (Choung et al., 2013).

coefficient	[a]EH36	DH36
α	3.72×10^5	5.56×10^4
β	9.40×10^6	8.54×10^6

Note:
[a] Applied for single beam model.

6. Conclusions

This study presents experimental and numerical investigations on the response of beams of low-temperature steel (LT-FH32) under a single impact and repeated impacts at a sub-zero temperature and room temperature, respectively. Seven identical impacts were repeatedly applied using a striker with a knife-edge header dropped from the same drop height throughout the impacts. Two models were tested at room temperature, and the other two were tested at the sub-zero temperature (approximately −50 °C). In the numerical study, strain hardening was considered by using the tensile test results and strain-rate hardening was considered by adopting the Cowper–Symonds constitutive equation along with the material constant proposed by other researchers. In addition, after validating the numerical analysis model against the tested data, further computations were also performed to gain insight into the collision forces and rebound velocity of the striker during impact and the effect of different impact positions, materials, and boundary conditions. From the results of this study, the following conclusions may be drawn:

- The material properties of low-temperature steel were obtained through tensile tests at various temperature levels, considering room temperature, −30, −50, and −70 °C. Yield strength, tensile strength, and strain gradually increased with decreasing temperature.
- The permanent deflections at the sub-zero temperature are smaller than those of the room temperature tests; this was also confirmed by Min et al. (2013) and Cho et al. (2014).
- The maximum permanent deflections of the beam significantly increased with increasing number of impacts regardless of impact velocity. However, the increment of maximum permanent deflections decreased with increasing number of impacts,

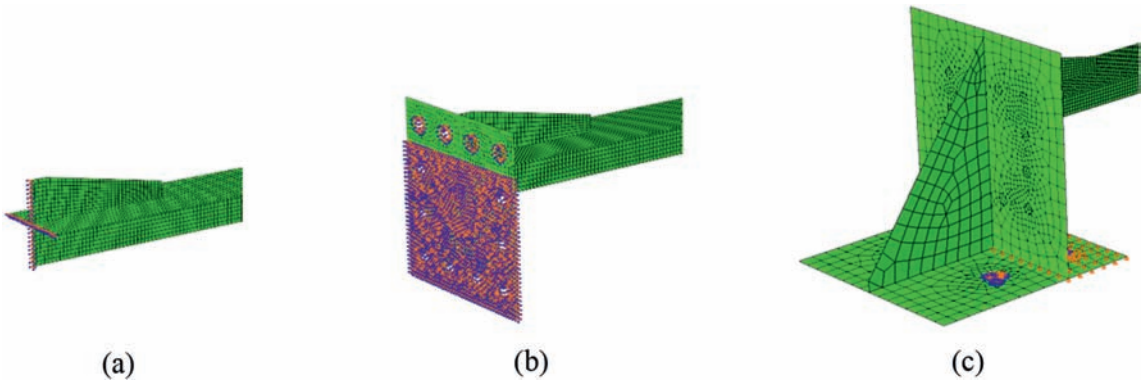

Fig. 18. Variations of boundary conditions: (a) Beam only (case 1), (b) Beam with endplate (case 2), (c) Beam with endplate and fixture (case 3).

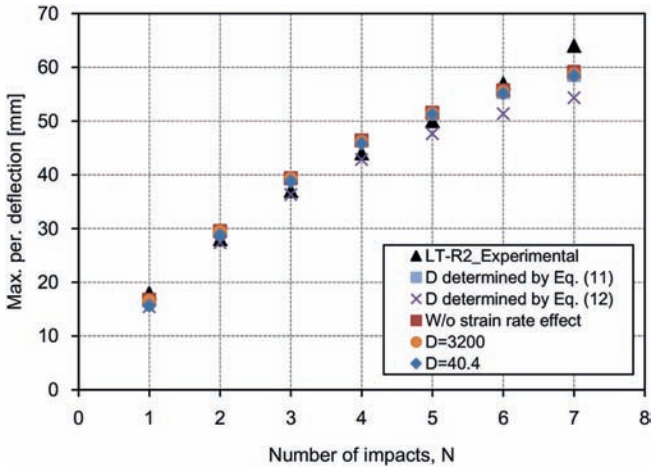

Fig. 20. Effect of strain-rate hardening definitions on a maximum permanent deflection of model LT-R2.

in which they decreased faster in the case of the lower impact velocity than in the higher impact velocity case.

- The numerical analysis model developed in this study can predict the permanent deflections of beam structures subjected to repeated lateral impacts at room temperature and a single impact at sub-zero temperatures with reasonable agreement.
- As the number of impacts increases, the maximum contact force increases but the impact duration decreases significantly. In other words, when the number of impacts increases the material can recover the elasticity; this was confirmed by Huang et al. (2000).
- Smaller deflections can be observed when the impact location is near the supports owing to the higher stiffness of the impact location, and smaller rotations occur, resulting in decreased deflection of the beam.
- The numerical simulation results are very sensitive to the means by which the supports are modelled. As expected, the full model similar to the experimental models gives a better prediction of the plastic behaviour of the beam under repeated mass impacts.
- The effect of strain rate hardening is numerically investigated. It is observed that in this particular study, the strain rate hardening definition considering coefficient of Cowper-Symonds equation, D as a constant during impact, was insignificantly affected to the accuracy of numerical simulations. However, when the method of predicting D that varied with true plastic strain was applied, underestimation of deflection was observed for all impact events, and the maximum permanent deflection and its increment were considerably decreased.

The investigation results of this study can be applied to the structural design of marine structures subjected to lateral mass impacts. However, further investigation seems to be necessary, especially on the effects of the repetition of impact loadings and sub-zero temperatures for severe impacts causing the fracture of impacted structures.

Acknowledgements

This work was supported by the Korea Institute of Energy Technology Evaluation and Planning, the Ministry of Trade, Industry and Energy of the Republic of Korea (No. 20154030200970).

References

ABAQUS, 2010. User's Manual Version 6.10.
Cerik, B.C., Shin, H.K., Cho, S.R., 2015. On the resistance of steel ring-stiffened cylinders subjected to low-velocity mass impact. Int. J. Impact Eng. 84, 108–123.
Chae, G.I., 2008. Nonlinear Structural Behavior Due to Repeated Interaction between Ice Breaking Commercial Ships and Sea Ice (Master thesis). School of Naval Architecture and Ocean Engineering, University of Ulsan, Ulsan, Korea.
Cho, S.R., Choi, S.I., Son, S.K., 2015. Dynamic material properties of marine steels under impact loadings. In: Proceedings of the 2015 World Congress on Advances in Structural Engineering and Mechanics, ASEM15. Incheon, Korea.
Cho, S.R., Kim, J.M., Kim, Y.H., 2011. Effect of design parameters of double hull side structures on their collision resistance. In: Proceedings of 25th Asian-Pacific Technical Exchange and Advisory Meeting on Marine Structures, Incheon, Korea, pp. 352–360.
Cho, S.R., Seo, B.S., Cerik, B.C., Shin, H.K., 2013. Experimental and numerical investigations on the collision between offshore wind turbine support structures and service vessels. In: Proceedings of the International Conference on Collision and Grounding of Ships and Offshore Structures. Trondheim, Norway, pp. 281–287.
Cho, S.R., Truong, D.D., Shin, H.K., 2014. Repeated lateral impacts on steel beams at room and sub-zero temperatures. Int. J. Impact Eng. 72, 75–84.
Choung, J., Nam, W., Lee, J.Y., 2013. Dynamic hardening behaviors of various marine structural steels considering dependencies on strain rate and temperature. Mar. Struct. 32, 49–67.
Cowper, G.R., Symonds, P.S., 1957. Strain-hardening and Strain-rate Effects in the Impact Loading of Cantilever Beams. Technical Report, No. 28. Division of Applied Mathematics, Brown University.
Dieter, G.E., 1986. The tension test. In: Bever, M.B., Copley, S.M., Shank, M.E., Wert, C.A., Wilkes, G.L. (Eds.), Mechanical Metallurgy, third ed. McGraw-Hill, New York, pp. 275–295.
Henchie, T.F., Chung Kim Yuen, S., Nurick, G.N., Ranwaha, N., Balden, V.H., 2014. The response of circular plates to repeated uniform blast loads: an experimental and numerical study. Int. J. Impact Eng. 74, 36–45.
Huang, Z.Q., Chen, Q.S., Zhang, W.T., 2000. Pseudo-shakedown in the collision mechanics of ships. Int. J. Impact Eng. 24, 19–31.
IMO, 1993. The International Code for the Construction and Equipment of Ships Carrying Liquefied Gases in Bulk. International Maritime Organization.
KS, KS B 0801, 2007. Test Pieces for Tensile Test for Metallic Materials. Korean Agency for Technology and Standard.
Lee, H.J., Kim, S.B., 2007. A study on application of material properties in ship collision analysis. In: Proceedings of the Annual Autumn Conference of the Social of Naval Architecture of Korea, Jeju, Korea, pp. 1050–1070 (in Korean).
Liu, B., Villavicencio, R., Guedes Soares, C., 2013. Experimental and numerical plastic response and failure of pre-notched transversely impacted beams. Int. J. Mech. Sci. 77, 314–332.
Min, D.K., Heo, Y.M., Shin, D.W., Kim, S.H., Cho, S.R., 2013. On the plastic and fracture damage of polar class vessel structures subjected to impact loadings. In: Proceedings of the International Conference on Collision and Grounding of Ships and Offshore Structures. UK, pp. 213–220.
Minamoto, H., Seifried, R., Eberhard, P., Kawamura, S., 2011. Analysis of repeated impacts on a steel rod with visco-plastic material behavior. Eur. J. Mech. A/Solids 30, 336–344.
Seifried, R., Schiehlen, W., Eberhard, P., 2005. Numerical and experimental evaluation of the coefficient of restitution for repeated impacts. Int. J. Impact Eng. 32, 508–524.
Villavicencio, R., Guedes Soares, C., 2011. Numerical modeling of the boundary conditions on beams struck transversely by a mass. Int. J. Impact Eng. 38, 384–396.
Villavicencio, R., Guedes Soares, C., 2012a. Numerical plastic response and failure of a pre-notched transversely impacted beam. Ships Offshore Struct. 7 (4), 417–429.
Villavicencio, R., Guedes Soares, C., 2012b. Numerical modelling of laterally impacted plates reinforced by free and end connected stiffeners. Eng. Struct. 44, 46–62.
Villavicencio, R., Kim, Y.H., Cho, S.R., Guedes Soares, C., 2013. Deformation process of web girders in small-scale tanker double hull structures subjected to lateral impact. Mar. Struct. 32, 84–112.
Zhu, L., Faulkner, D., 1996. Damage estimate for plating of ships and platforms under repeated impacts. Mar. Struct. 9, 697–720.